The Astrophysical Journal, 844:51 (10pp), 2017 July 20 https://doi.org/10.3847/1538-4357/aa7bef

Decay of Solar Wind Turbulence behind Interplanetary Shocks

Alexander Pitňa[1], Jana Šafránková[1], Zdeněk Němeček[1], and Luca Franci[2]
[1] Charles University, Faculty of Mathematics and Physics, V Holesovickach 2, Prague, CZ-18000, Czech Republic; offelius@gmail.com
[2] Dipartimento di Fisica e Astronomia, Universita degli Studi di Firenze, I-50125 Firenze, Italy
Received 2017 April 6; revised 2017 June 3; accepted 2017 June 24; published 2017 July 21

Abstract

We investigate the decay of magnetic and kinetic energies behind IP shocks with motivation to find a relaxation time when downstream turbulence reaches a usual solar wind value. We start with a case study that introduces computation techniques and quantifies a contribution of kinetic fluctuations to the general energy balance. This part of the study is based on high-time (31 ms) resolution plasma data provided by the Spektr-R spacecraft. On the other hand, a statistical part is based on 92 s Wind plasma and magnetic data and its results confirm theoretically established decay laws for kinetic and magnetic energies. We observe the power-law behavior of the energy decay profiles and we estimated the power-law exponents of both kinetic and magnetic energy decay rates as −1.2. We found that the decay of MHD turbulence does not start immediately after the IP shock ramp and we suggest that the proper decay of turbulence begins when a contribution of the kinetic processes becomes negligible. We support this suggestion with a detailed analysis of the decay of turbulence at the kinetic scale.

Key words: plasmas – shock waves – solar wind – turbulence

1. Introduction

Magnetohydrodynamic (MHD) turbulence is present in many areas of physics, ranging from industrial applications of fluids, through nuclear fusion to plasma physics, including astrophysical and solar physics. An observed number of MHD flow types in different plasma environments leads to the question of universality of MHD turbulence, which has been a subject of intensive research (e.g., Servidio et al. 2008; Grappin & Müller 2010; Boldyrev et al. 2011; Linkmann et al. 2015). In the solar wind, a correlation of the different vector fields could influence the energy transfer from larger to smaller scales (e.g., Biskamp 1993), thus turbulent processes control the amount of energy that is dissipated at small scales with consequences for heating rates.

The core solar wind protons are observed to be heated perpendicularly to the magnetic field (e.g., Marsch et al. 1983; Hellinger et al. 2013), and also a preferential heating of minor ions was registered (e.g., von Steiger et al. 1995; Hefti et al. 1998; Cranmer et al. 1999, 2008). The dissipation of the turbulent energy cascade can partially account for heating of the protons leading to nearly isothermic solar wind expansion (e.g., Verma et al. 1995; Vasquez et al. 2007; Coburn et al. 2012; Lamarche et al. 2014). The interplanetary medium exhibits velocity and magnetic field fluctuations that reflect properties consistent with a turbulent cascade (e.g., Coleman 1968; Bavassano et al. 1982; Matthaeus et al. 1982; Smith et al. 2006). MHD simulations show that turbulence produces mostly highly oblique (quasi-2D), low-frequency fluctuations (e.g., Zank & Matthaeus 1993; Goldreich & Sridhar 1995; Matthaeus et al. 1996, 1998; Müller & Grappin 2005; Beresnyak 2011; Oughton et al. 2013).

The solar wind is compressible and inhomogeneous at larger scales. Large-scale inhomogeneities, such as velocity shear layers or temperature and density gradients, can supply energy to the small-scale turbulence. The observed fluctuations are broadband with correlation scales around 0.02 au at Earth orbit that are much smaller than the scale of the system (1 au or more). The MHD turbulence inertial range extends roughly down to scales of 1000 times smaller, near the thermal ion gyroscale (Zhou et al. 2004). Thus, turbulence activity is well separated in a length scale from the large-scale solar wind inhomogeneities. Moreover, the large-scale properties, such as mean flow and magnetic field, are relatively coherent and reproducible. In contrast, the observed small-scale solar wind fluctuating fields are generally viewed as random and locally homogeneous. These fluctuations were treated originally using linearized weakly inhomogeneous MHD (e.g., Parker 1965; Hollweg 1978, 1986; Barnes 1979), which describes a propagation of short-wavelength Alfvénic fluctuations in an inhomogeneous flow. The present view suggests that the solar wind is locally incompressible (Matthaeus et al. 1990) and can be described as MHD turbulence with an acceptable degree of approximation.

As a turbulent plasma (e.g., Goldstein et al. 1995; Horbury et al. 2005; Alexandrova et al. 2013; Bruno & Carbone 2013), the solar wind variations have a power spectrum extending over many orders of magnitude (e.g., Coleman 1968). Scales larger than the ion gyroradius or inertial length of the protons are known as the inertial range, and the spectral indices at 1 au are observed to be close to $-5/3$ for the magnetic field and density, and $-3/2$ for the electric field and velocity (e.g., Matthaeus et al. 1982; Bale et al. 2005; Podesta et al. 2007; Podesta & Borovsky 2010; Chen et al. 2011). Magnetic spectra are variable and ion instabilities occur as a function of the local plasma parameters. There is also evidence that the fluctuations are predominantly Alfvénic (e.g., Belcher & Davis 1971; Horbury et al. 1995; Bale et al. 2005; Chen et al. 2011). At larger frequencies around ion scales, the spectra exhibit a break followed-up local flattening (e.g., Chandran et al. 2009; Šafránková et al. 2013b).

A small-scale turbulent cascade of the magnetic energy from proton scales, where kinetic properties of ions do not meet fluid approximations, is characterized by a steeper power-law spectrum of magnetic and density fluctuations with a spectral index close to −2.8 (e.g., Leamon et al. 1998; Smith et al. 2006; Alexandrova et al. 2008, 2009; Sahraoui et al. 2009; Chen et al. 2012, 2014; Bruno & Carbone 2013; Howes 2015;

Riazantseva et al. 2015; Šafránková et al. 2015). At these scales, turbulent fluctuations become more compressible (Leamon et al. 1998; Alexandrova et al. 2008; Chen et al. 2012; Salem et al. 2012; Kiyani et al. 2013). Franci et al. (2015) explained a switch in the spectral slopes as a result of the natural continuation of a large-scale MHD turbulent cascade through proton and down to electron scales, where couplings of the different fields are governed by the non-ideal terms of the Ohm law.

On the other hand, the spectral slope of velocity fluctuations very close to $3/2$ was confirmed by many authors who used different spacecraft data and various techniques of a spectral analysis (Podesta et al. 2006, 2007; Salem et al. 2007; Podesta & Borovsky 2010; Chen et al. 2011, 2013). Recently, the statistics of Šafránková et al. (2016) has shown that the median slopes of the bulk speed of the segment attributed to the MHD scale is -1.43, whereas it is -3.08 in the kinetic range.

In MHD turbulence, differential equations that govern the decay of energy, E were derived by Biskamp (2003). Solutions of these equations lead to power laws, $E \approx (t - t_0)^n$ where the power-law exponent, n determines how quickly the turbulent energy decays. However, the total energy is a sum of kinetic and magnetic energies, $E = E_k + E_b$ and each of them could decay with a different rate. Biskamp & Müller (1999) showed that in the case of finite magnetic helicity, the decay rates of magnetic and kinetic energies are $E_b \propto t^{-1/2}$ and $E_k \propto t^{-1}$, respectively. Therefore, a ratio of the kinetic and magnetic energies, r_A is not constant in time, implying that the dynamics of turbulence in the inertial range is not controlled by the Alfvén wave effect (Biskamp & Müller 2000).

The key to understand an MHD turbulence decay is to identify relevant timescales, how they are influenced by anisotropy associated with a large-scale magnetic field, and how a balance between nonlinear distortions and the sweep-like dynamics associated with wave propagation is spread out (Zhou et al. 2004). In the simplest MHD case where incompressibility, isotropy, stationarity, and homogeneity are assumed, two magnetic and velocity fields and Alfvén wave propagation effects play a role. There are two classes of timescales suggested (Matthaeus & Zhou 1989): the nonlinear time and the Alfvén time (the time for propagation of a fluctuation in a given length scale). Moreover, the large-scale magnetic field introduces a preferred direction and anisotropic effects are present.

An optimal to investigate the energy decay laws in the solar wind is to use an in-line configuration of three or more spacecraft because a radial expansion of the solar wind and the decay of turbulent fluctuations can be studied directly (Bruno et al. 2009). Another possibility is to analyze data from a spacecraft moving radially to (or from) the Sun, which observes the same plasma stream at different heliocentric distances (Bavassano et al. 1982). However, these investigations are rare and difficult because they require a special configuration of the spacecraft. We suggest a novel approach that is based on an analysis of turbulence behind interplanetary (IP) shocks that can be encountered in the solar wind rather often. Note that their occurrence rate depends on the solar cycle and it can be as high as one shock per day (Webb & Howard 2012). After the IP shock passage (in the downstream region), the power of the turbulent fluctuations is enhanced approximately 10 times relative to its upstream values (Luttrell et al. 1984; Lu et al. 2009; Hu et al. 2013; Pitňa et al. 2016).

Although IP shocks have been intensively studied for decades and many aspects of shock physics are understood (e.g., Balogh & Treumann 2013), some open questions connected with turbulence remain. At IP shocks, the upstream bulk energy is likely dissipated into turbulent waves, which in turn heat the downstream plasma and transfer energy to suprathermal ions and electrons into the downstream region. These processes depend on the characteristic spatial scales at the shock transition region (e.g., Lee et al. 1986; Scholer et al. 2003). Based on the energy containing model, Zank et al. (2002) investigated the amplification of turbulence by the shock and variations in the shock velocity and the shock thickness induced by the presence of upstream turbulence, the destabilization of the shock by turbulence, and the rate at which downstream transmitted turbulence decays as it is convected away from the shock. They found that for a steady shock, a turbulent energy density decays with an $\approx t^{-2/3}$ dependence in the downstream region. Lu et al. (2009) discussed enhanced amplitudes (10–30 times) of the upstream Alfvén waves transmitted into the downstream region.

Adhikari et al. (2016a, 2016b) simplified a set of equations governing the interaction of turbulence with the shock wave (Zank et al. 2012) and compared results of theoretical considerations with observations of both quasiperpendicular and quasiparallel IP shocks. The authors note an increase of the turbulent energy across the shock and its gradual decrease downstream. They predominantly studied shocks with weak or moderate strength and they found that the increase of the turbulent energy from upstream to downstream was larger for stronger shocks. Surprisingly, no significant difference in the behavior of the total turbulent energy and its components was found between quasiperpendicular and quasiparallel IP shocks.

To clarify, the influence of IP shocks on plasma turbulence in the frequency range covering a transition from MHD to kinetic scales, Pitňa et al. (2016) focused on changes of the level of ion flux fluctuations and variations of their spectral properties upstream and downstream of fast forward oblique interplanetary shocks. The authors have shown that (1) the level of ion flux fluctuations in both MHD and kinetic ranges increases by a factor larger than 10 across fast forward IP shocks; (2) the ratio of PSDs in the downstream and upstream regions exhibits a clear peak at the frequency that can be associated with the break between MHD and kinetic scales; and (3) spectral indices of both MHD and kinetic scales in the downstream are proportional to the corresponding values of the indices in upstream regions with correlation coefficients of about 0.75 and 0.8 in MHD and kinetic ranges, respectively. This indicates that properties of the turbulent cascade are conserved across the shock.

In the paper, we investigate the decay of both magnetic and kinetic energy constituent downstream IP shocks in order to find a relaxation time when downstream turbulence reaches values close to upstream conditions. We start with a case study that introduces computation methods and quantifies a contribution of kinetic fluctuations to the overall energy balance. This part of a study is based on high-time resolution data provided by the Spektr-R spacecraft and it is followed by the extended statistical analysis that uses Wind plasma and magnetic field observations with a time resolution of 92 s. Statistical results confirm the earlier theoretically established decay laws for kinetic and magnetic energies. However, we found that the decay of MHD turbulence does not start immediately after the IP shock ramp. We suggest

that this delay is connected with kinetic processes behind the shock ramp that increases a level of MHD turbulence (e.g., Luttrell et al. 1984; Lu et al. 2009; Pitňa et al. 2016). The proper decay of turbulence thus starts when a contribution of these processes becomes negligible. We support this suggestion by an analysis of the decay of turbulence at the kinetic scale that is presented in the last part of the paper.

2. Data Processing

Central to the issue of the turbulent cascade is the idea of a spectral energy transfer. At any wave number, k in the inertial range, there is an energy transfer mechanism that pumps the energy into higher wave numbers. The timescale associated with this transfer $\tau_T(k)$ depends on the wave number, k, and turbulent scenario under consideration (Zhou et al. 2004). We assume that solar wind turbulence is moderately anisotropic and strain-dominated. In this framework, the spectral energy transfer time can be expressed as $\tau_T(k) = 1/(ku(k))$, where $u(k)$ presents the root mean square of velocity fluctuations at wave number, k (Zhou et al. 2004).

Under the assumptions that (a) the IP shock propagates into a stationary and homogenous medium and (b) a solar wind expansion is not significant over the spatial scales of interest, we can consider the profiles of downstream magnetic field and plasma parameters as a demonstration of a decay of the open turbulent system. Since the analysis is based on an evaluation of changes of the turbulent energy in time, we should determine the proper timescale. Let us set the time of the shock ramp observation to zero, then the plasma that is observed at a time t_{sp} behind the shock passage was shocked at a time $t_{sh} \geqslant t_{sp}$. The expression for t_{sh} can be easily derived when a frame of reference where the downstream plasma is at rest is used

$$t_{sh} = t_{sp} K. \tag{1}$$

The constant, K can be written as

$$K = \frac{v_{sh}}{v_{sh} - \boldsymbol{v}_d \cdot \boldsymbol{n}}, \tag{2}$$

where v_{sh} is the IP shock speed in the spacecraft frame of reference, $\boldsymbol{v}_d$ is the mean downstream solar wind speed observed at the spacecraft, and $\boldsymbol{n}$ is the shock normal. The value of the constant K is a characteristic of each particular IP shock.

As we mentioned above, the relevant timescale for the MHD decay is the spectral transfer time, τ_T, that would serve as a unit of the time, t_{sh}. We approximate it with the eddy turnover time, $\tau_{nl}(k)$ (e.g., Franci et al. 2015), and we estimate τ_{nl} from solar wind velocity measurements as

$$\tau_{nl} = \frac{\langle |\boldsymbol{v}_d| \rangle_{\delta t}\, \delta t}{2\pi \sqrt{\sum_{i=0}^{2} \mathrm{var}_{\delta t}(v_{d,i})}}, \tag{3}$$

where $\langle\rangle_{\delta t}$ and $\mathrm{var}_{\delta t}$ denote the mean and variance of a physical quantity on a timescale δt, respectively, and $v_{d,i}$ stands for velocity components ($i = 0, 1, 2$). Here, we used Taylor's (1938) hypothesis, which allows us to express a wave number as $k = 2\pi/v_d \delta t$.

Putting Equations (1) and (3) together, we can recalculate the time t_{sp} into the dimensionless time, t_{nl}, that reflects a propagation (usually oblique) of the shock in the solar wind frame (Equation (1)) and that is expressed in units of the eddy turnover time τ_{nl} (Equation (3)):

$$t_{nl} = \frac{t_{sp} K}{\tau_{nl}}. \tag{4}$$

Finally, we estimate the kinetic, E_k, and magnetic, E_b, energies from the measurements of the density, ρ, solar wind velocity components, v_i, $i = 0, 1, 2$, and magnetic field components, B_i, $i = 0, 1, 2$, as

$$\boldsymbol{E}_k = \frac{1}{2} \langle \rho \rangle_{\delta t} \sum_{i=0}^{2} \mathrm{var}_{\delta t}(\boldsymbol{v}_i) \tag{5}$$

and

$$\boldsymbol{E}_b = \frac{1}{2\mu_0} \sum_{i=0}^{2} \mathrm{var}_{\delta t}(\boldsymbol{B}_i), \tag{6}$$

where μ_0 is the permeability of the vacuum.

3. Data Used

As we noted in the first section, we present an example of the evolution of velocity fluctuations behind one IP shock and later we perform a statistical analysis of the decay of turbulent energy and its components, E_k and E_b. In the example, we use high-resolution data from a monitor of solar wind parameters, BMSW (Bright Monitor of the Solar Wind) on board Spektr-R (Šafránková et al. 2013a; Zastenker et al. 2013). The instrument can operate either in adaptive or sweep modes, which differ with a time resolution of the density, thermal, and bulk solar wind speeds. The former mode measures with a cadence of 31 ms, while the latter mode with the cadence of 1–3 s. Here, we present the data measured in the adaptive mode downstream of the IP shock.

A large statistical study is based on the data from the Solar Wind Experiment (SWE) and Magnetic Field Investigation (MFI) instruments (Lepping et al. 1995; Ogilvie et al. 1995) on board Wind. The cadence of measurements is much lower than that of BMSW, namely 92 s for SWE and ≈0.1 s for MFI. The main reason for an application of WIND measurements is a significantly larger number of IP shocks detected by the spacecraft, and simultaneous measurements of plasma parameters and magnetic field. We used IP shock parameters from the Heliospheric Shock Database generated and maintained at the University of Helsinki (http://ipshocks.fi/database). The criteria for a selection were (1) the velocity jump exceeding 20 km s^{-1} and (2) a sufficiently long (minimum 10 hr) downstream interval without data gaps and large disturbances like consecutive shocks. The final data set includes 174 fast forward IP shocks that were detected between 2006 January 1 and 2015 September 22.

The timescale δt that we chose in our study is 30 minutes, which is large enough to estimate kinetic and magnetic energies in the inertial range and small enough to capture the fast energy decay behind IP shocks. The first sample starts 2 minutes after the shock ramp and the next one is shifted by 5 minutes, i.e., the consecutive samples are overlapped by 25 minutes. Note that these numbers refer to the spacecraft time.

For each shock, we computed the constant K and the eddy turnover time, τ_{nl} using Equations (2) and (3). The turnover time depends on the spatial dimensions of eddies that are represented by δt in Equation (3). Since the power spectral density (PSD) of turbulent fluctuations decreases with the

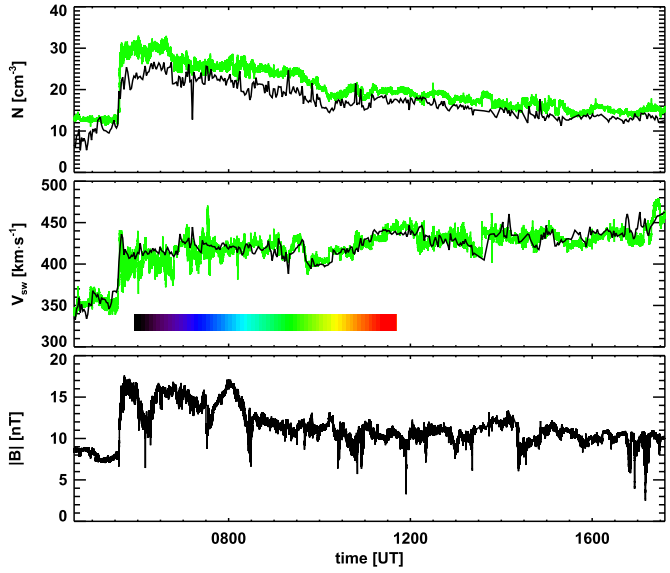

Figure 1. Example of the IP shock registered on 2015 June 22 by Spektr-R and Wind. The upper and middle panels show time profiles of the density, N and solar wind speed, V_{SW}, respectively. The black color presents the data from SWE (Wind) and the green color marks the data from BMSW (Spektr-R). The bottom panel presents the magnetic field strength from MFI (Wind). A color bar in the middle panel codes the time that will be used in several subsequent figures.

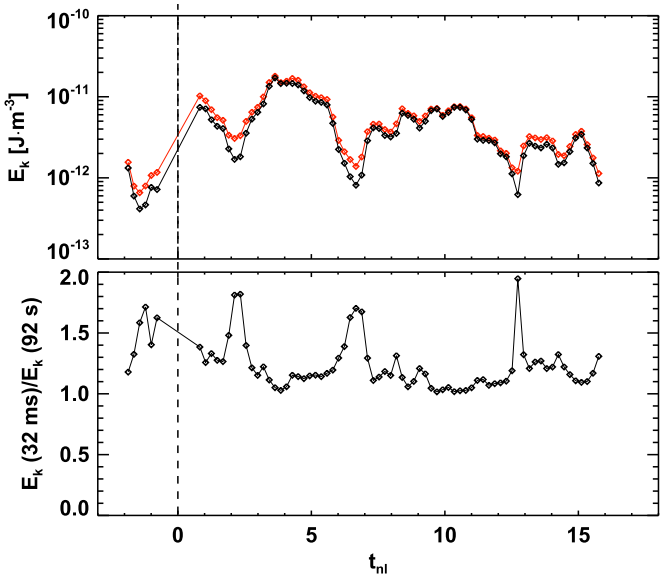

Figure 2. Demonstration of a contribution of small-scale variations to the kinetic component of turbulent energy. Top panel: red points are computed with full time resolution, the black points stand for the kinetic energy computed from the 92 s averages. Bottom panel: a ratio of profiles from the top panel.

frequency (or with characteristic dimensions of the eddies), the dominant portion of the turbulent energy contains the largest eddies. For this reason, we chose δt equal to the duration of our samples. To simplify the analysis, we use τ_{nl} determined for the first sample through a whole downstream interval of each particular IP shock and approximate the nonlinear time, t_{nl} according to Equation (4). Finally, we apply Equations (5) and (6) to compute kinetic, E_k and magnetic, E_b energies, respectively.

4. Case Study

As an example of the analysis, we present the IP shock that was detected by BMSW on 2015 June 22 at 0536 UT (0505 UT at Wind). Figure 1 presents measurements of the density, solar wind speed, and magnetic field strength 1 hr upstream and 12 hr downstream of this IP shock. The basic parameters of the shock are the magnetosonic Mach number, $M_{ms} = 2.6$, the angle between the shock normal and upstream magnetic field, $\theta_{Bn} = 78°$, the shock speed in the spacecraft frame, $v_{sh} = 483$ km s^{-1}, the ratio of the downstream to upstream densities, $\rho_d/\rho_u = 1.8$, the difference between downstream and upstream solar wind speeds (in the spacecraft frame), $v_d - v_u = 60$ km s^{-1}, and a ratio between downstream and upstream magnitudes of the magnetic field, $B_d/B_u = 1.7$. A conversion factor between the spacecraft time, t_{sp} and nonlinear time, t_{nl} was 2.5 s^{-1} in this particular case.

The green profiles in Figure 1 correspond to Spektr-R plasma measurements, whereas Wind observations are shown in black. Note that magnetic field measurements are available only on board Wind but an excellent matching of Spektr-R and Wind plasma observations demonstrated in the first two panels suggests that the data from these two sources can be combined. The reason for this combination is the time resolution. As already noted, the Spektr-R time resolution allows for investigations of the evolution of the velocity turbulent cascade down to ion kinetic scales, but there are no magnetic field measurements.

The evolution of the Spektr-R kinetic energy as a function of the time (in units of the eddy turned time, τ_{nl}, with $t_{nl} = 0$ for the IP shock passage) is shown in Figure 2. The red points use a full time resolution (Spektr-R) of velocity measurements, whereas 92 s mean values (Wind time resolution) were used for the black points. A ratio of these profiles is plotted in the bottom panel. This ratio is always larger than unity but it stands near the value 1.2 for most of the time with several excursions to 1.8. These excursions are rare and would ideally analyze the energy decay over one order of magnitude, thus we could limit ourselves to the Wind time resolution.

Figure 2 shows about 10 hr of downstream measurements and one would expect to observe a significant decrease of the turbulent energy over this course of time. The energy exhibits a slightly decreasing overall trend but this trend is hidden in large variations. For this reason, Figure 3 presents the data filtered by the floating median. The red and black lines show the magnetic and kinetic energies, respectively, computed from Wind, and the green line stands for the kinetic energy computed from the Spektr-R velocity. A relatively good matching of green and black profiles until $t_{nl} \approx 15$ indicates that both spacecraft observed the same solar wind stream, but they were probably located in different flux tubes later. For this reason, the Alfvén ratio in the lower panel is computed from Wind. The upper panel shows a decrease of both kinetic and magnetic energies in time but this decrease is not monotonic; rather, an increase is seen at the beginning, and both energies are about constant until $t_{nl} \approx 9$. The Alfvén ratio is fluctuating at the beginning and it stabilizes at a level of 0.4 at the end of the interval in this particular case. In order to determine if these features are typical, we performed a statistical study, which is described in the next section.

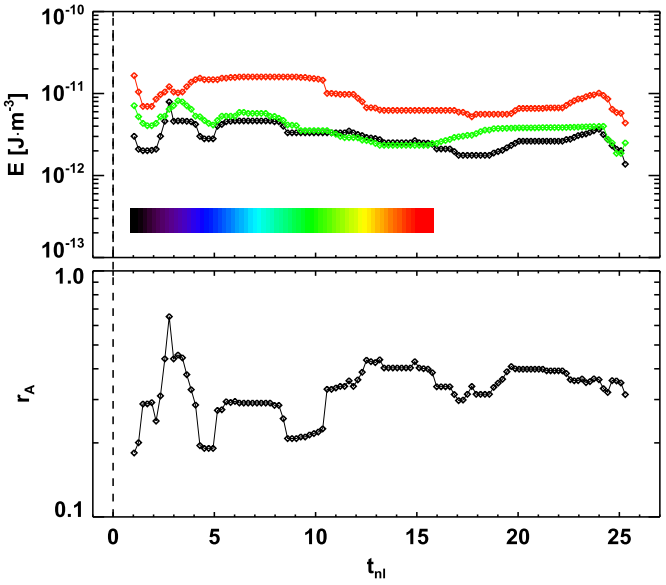

Figure 3. Comparison of magnetic, E_M (red-Wind), and kinetic, E_K, energies (black-Wind, green-Spektr-R) behind the IP shock in Figure 1. The x-axis represents the time expressed in units of the eddy turnover time, $\tau_{\rm nl}$, with $t_{\rm nl} = 0$ at the shock passage. A color bar repeats the times from Figure 1.

5. Turbulence Decay: Statistical Study

Although the analysis of turbulence presented in the previous section is promising, the number of cases with high-time resolution of the plasma velocity from BMSW is too small. Thus, we focus on the MHD scale using a large set of IP shocks detected by WIND and perform a superposed epoch analysis. A set of 174 events consists of 133 quasiperpendicular and 41 quasiparallel fast forward shocks. Their magnetosonic Mach numbers range from 1.1 to 9 with the most probable value around 1.8.

A computation procedure was similar to that used for the case study and again we analyzed 10 hr downstream of each shock. The downstream energy levels of different shocks vary over more than a decade, thus we normalized kinetic and magnetic energy profiles to the values immediately downstream of the shock ($E_{\rm k,0}$, $E_{\rm b,0}$). We present these superposed normalized profiles for a whole set in a linear scale (upper panels) and in a log–log scale (lower panels) in Figure 4 (kinetic energy) and Figure 5 (magnetic energy). The red and blue diamonds mark the geometric averages of data points in logarithmically scaled time bins. The spread of individual points is large but the averages clearly show decreasing trends of both energies. However, the trend is not monotonic (similarly to the case study in the previous section). We observe an initial increase of both energies (up to $t_{\rm nl} \approx 2$) and a constant value up to $t_{\rm nl} \approx 10$; a decay is visible for larger times. For easier comparison of the trends of both energy profiles, we present them in Figure 6.

In order to make a rough quantitative estimate of the decay rates, we used a nonlinear least square fit using the Levenberg–Marquardt algorithm. The model function has the form

$$E(t_{\rm nl}) = \left(\frac{t_{\rm nl} - t_0}{t_{\rm d} - t_0}\right)^n, \qquad (7)$$

where $t_{\rm d} = 10$, t_0, and n are free parameters of the model. We adapted the Biskamp (2003) function with a motivation to account for the fact that the normalized energies start their

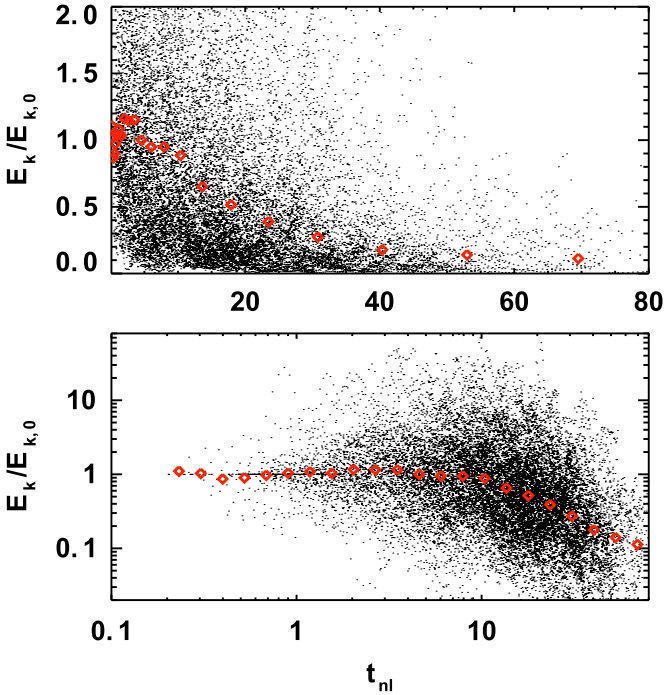

Figure 4. Superposed normalized $E_{\rm k}/E_{\rm k,0}$ profiles of all IP shocks. The data are displayed in a linear scale (upper panel) and a log–log scale (bottom panel). The red diamonds denote the geometric means in the logarithmically scaled time bins.

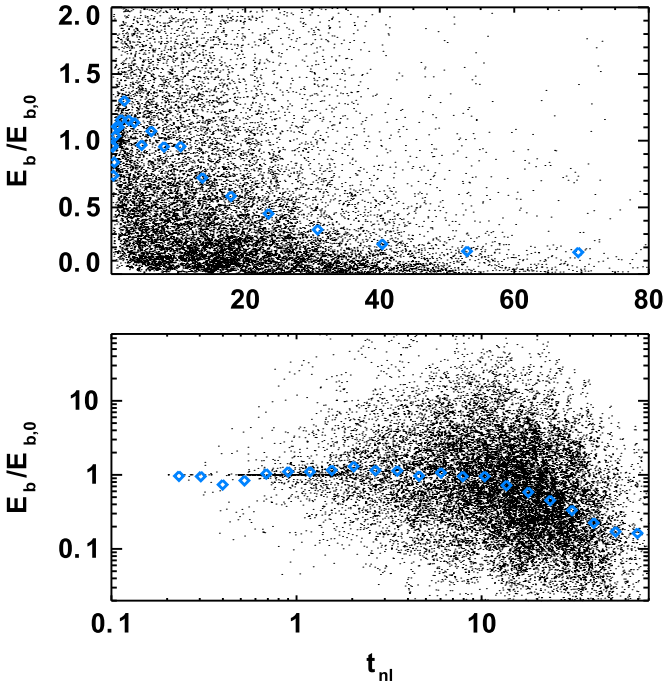

Figure 5. Superposed normalized $E_{\rm b}/E_{\rm b,0}$ profiles of all IP shocks. The data are displayed in a linear scale (upper panel) and a log–log scale (bottom panel). The blue diamonds denote the geometric means in the logarithmically scaled time bins.

decay approximately at $t_{\rm nl} = 10$ and that the values of $E_{\rm k}/E_{\rm k,0}$ and $E_{\rm b}/E_{\rm b,0}$ at this time are approximately equal to unity. This behavior can be clearly seen in Figure 6. In this figure, the blue line represents the best fit of the model function according to Equation (7) for the magnetic energy decay $t_0 = -4 \pm 2$ and

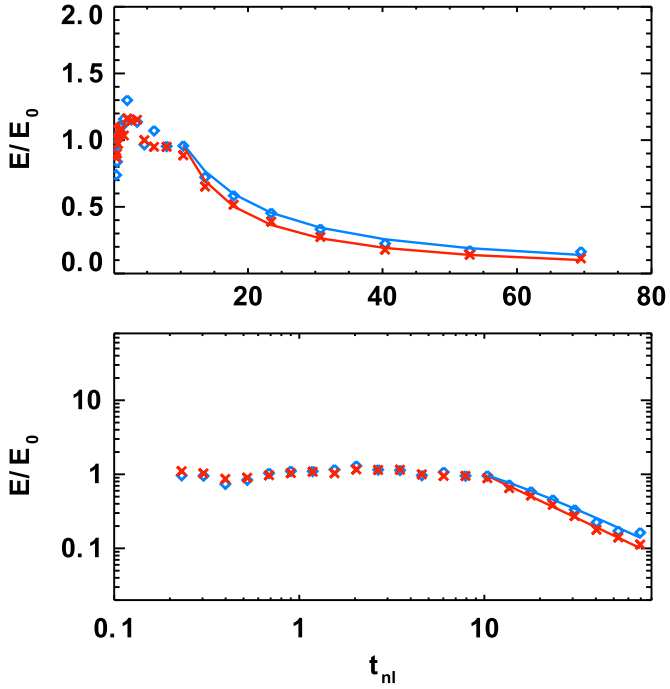

Figure 6. Normalized kinetic (red crosses) and magnetic (blue circles) energy profiles from Figures 4 and 5. The values are displayed in a linear scale (upper panel) and a log–log scale (bottom panel). The red and blue curves denote the best power-law model functions from the nonlinear least squares analysis. E/E_0 on the y axis denotes either $E_k/E_{k,0}$ or $E_b/E_{b,0}$.

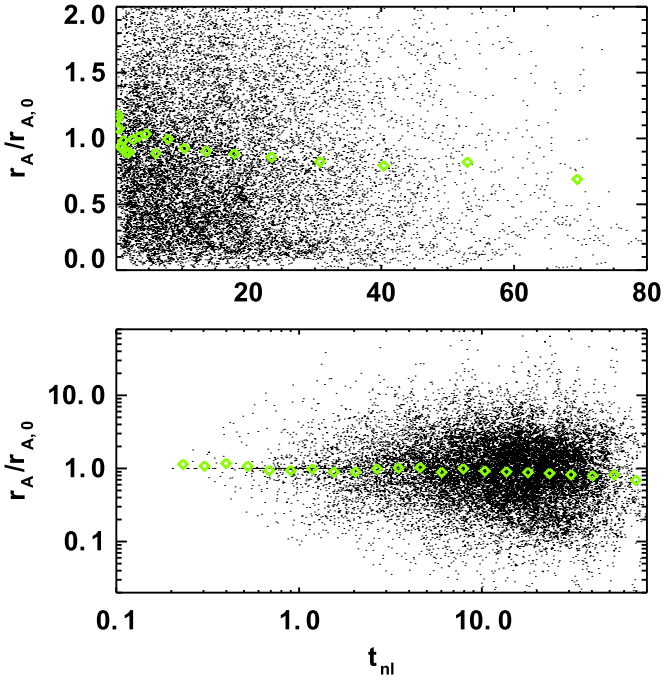

Figure 7. Superposed normalized Alfvén ratio profiles of all IP shocks. The data are displayed in a linear scale (upper panel) and a log–log scale (lower panel). The green diamonds show the geometric means in the logarithmically scaled time bins.

$n = -1.2 \pm 0.1$. The red line shows a similar fit for the kinetic energy decay with $t_0 = 0 \pm 2$ and $n = -1.2 \pm 0.1$.

For the sake of completeness, a superposed analysis of the Alfvén ratio profiles for our set of IP shocks is presented in Figure 7. Note that the Alfvén ratio profiles are normalized to their first downstream value for each profile. This ratio is about constant; a very weak declining trend that can be seen in the linear scale (upper panel) shows that the decay rate is slightly larger for the kinetic than for the magnetic component.

Equation (7) contains two characteristic times: t_d and t_0. The time, t_0, is an artificial parameter introduced by Biskamp et al. (2003) in order to account for the setting of a turbulent state in the simulation domains. The newly introduced parameter t_d expressed in units of t_{nl} stands for the time when a normalized energy is equal to unity and thus it has a meaning of the fluctuation amplitude. Although there is no clear physical reason, we followed the data in Figures 4 and 5 and we used identical values of t_d for both E_k and E_b.

6. Contribution of Kinetic Fluctuations to Turbulence Decay

We suggest that a source of the energy that compensates the natural decay of the turbulent energy until $t_{nl} \sim t_d$ is connected with the kinetic processes initiated at the shock. For this reason, we return to the shock shown in Figure 1 and analyze the kinetic range of turbulence. It should be noted that we combine Spektr-R velocity measurements with the Wind magnetic field data. As our previous analysis revealed (Figure 3), this combination can be used until $t_{nl} \approx 15$ but it is questionable for the later times.

We estimated the PSDs (traces of the power spectral matrix) of the downstream velocity, V_d, and magnetic field, B, variations first approximately 6 hr after the shock. We employ the

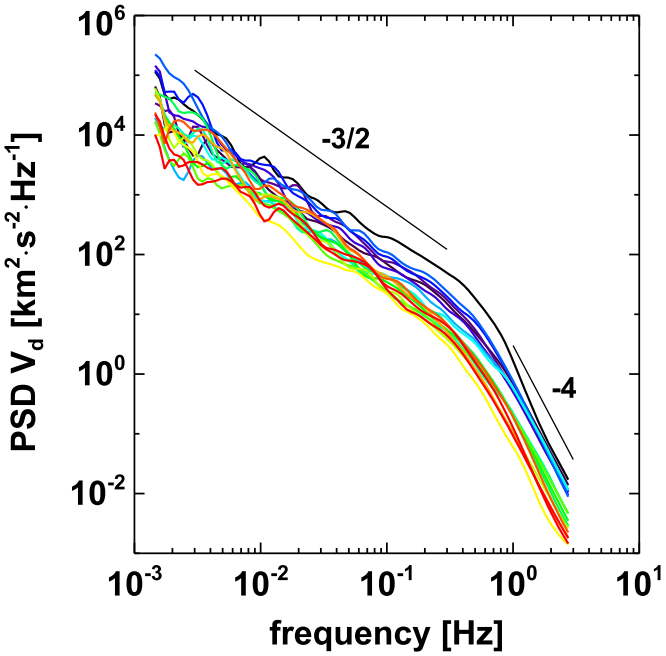

Figure 8. PSDs of velocity variations downstream of IP shock as a function of the frequency. The plasma data are from Spektr-R. Colors code the times downstream of the IP shock, according to Figure 1.

Continuous Wavelet Transform (CWT) algorithm using the Morlet mother function with $\omega_0 = 6$ (Torrence & Compo 1998). Figures 8 and 9 show the PSDs of V_d and B, respectively. In the figures, different colors mark time intervals over which the spectra were calculated (see the colored bar in Figures 1 and 3). The shapes of PSDs agree with the spectra already reported. In the inertial range, the slopes of PSD V_d and B in a log–log scale are around -1.5 and -1.65, respectively. Around $f \approx 0.5$ Hz,

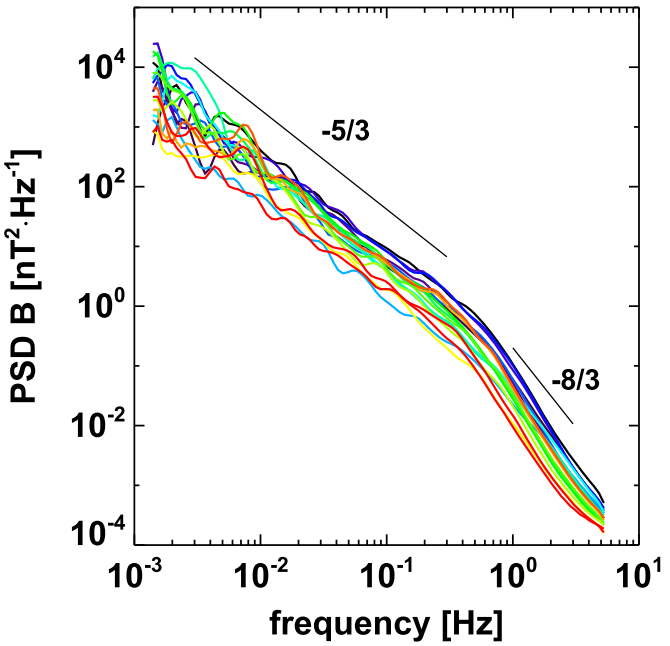

Figure 9. PSDs of magnetic field variations downstream IP shock as a function of the frequency. The data are from Wind. Colors code the times downstream of the IP shock, according to Figure 1.

there is a break in both PSDs, and the slopes of PSDs are steeper in the kinetic scale. Finally, we can see that the power within the fluctuations in the whole frequency range decreases with the time (see different colors of PSDs). For a better visualization of the evolution of PSD V_d and PSD B in time, a single value of PSD at ≈1 Hz was chosen and it is showed in Figure 10 as a function of t_{nl}. The level of fluctuations immediately downstream of the shock falls rapidly for about ≈10 τ_{nl} and then it becomes flat. This is true for both components of turbulent energy because Figure 11 shows that there is a clear correlation between the levels of magnetic and velocity fluctuations.

A comparison of Figures 3 and 10 reveals different behaviors of turbulence in the inertial and kinetic ranges. Whereas an MHD turbulence level is about constant for $t_{nl} < 10$ (see Figure 3), the level of kinetic turbulence decreases. This behavior is not clear from the time evolution of frequency spectra in Figures 8 and 9 because both the MHD and kinetic parts apparently exhibit a similar decrease over the depicted frequency range. However, magnetic and kinetic energies in Figure 3 are integrated quantities and the integration covers larger scales than those shown in Figures 8 and 9. Since PSDs of turbulent variations fall rapidly toward smaller scales, the integrated turbulent energy is determined by variations at the largest scales. The main purpose of Figures 8 and 9 is to demonstrate a decrease of the energy at the kinetic scale. Moreover, a closer examination of Figure 8 shows that the kinetic parts of the spectra are well ordered in time and the decrease of PSDs is nearly monotonic at all frequencies but it is not true for the MHD parts. It seems that the setting of an equilibrium starts from small scales and proceeds toward larger scales.

Our simple analysis cannot reveal underlying processes but this behavior resembles the inverse cascade that transfers the energy from smaller to larger scales. In this interpretation, the kinetic fluctuations enhanced at the shock transfer part of their energy to MHD fluctuations, and thus their levels do not

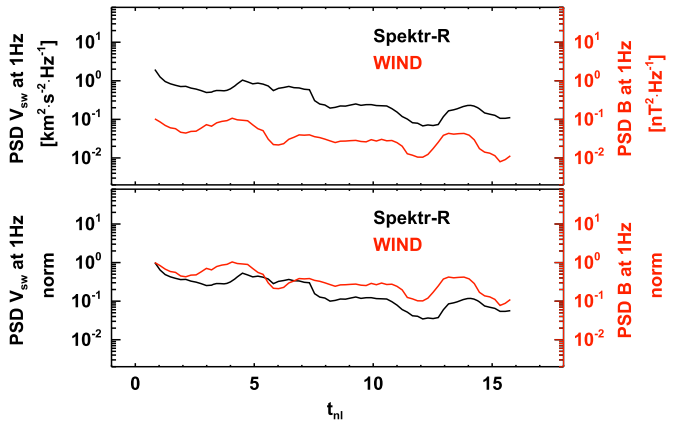

Figure 10. Evolution of the estimated PSDs of V_{sw} (black) and B (red) at 1 Hz as a function of the nonlinear time. In the bottom panel, the same profiles normalized to the values immediately downstream of the IP shock.

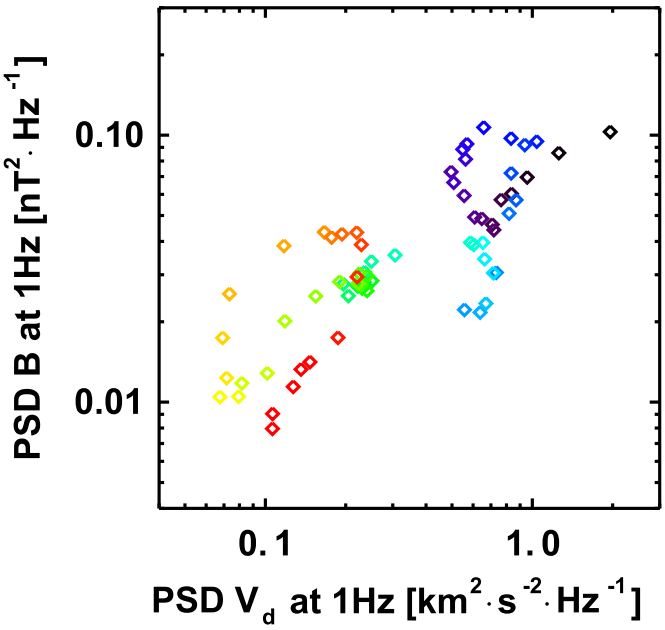

Figure 11. PSDs of magnetic fluctuations as a function of velocity fluctuations at 1 Hz. The values are taken from Figure 10 and colors represent the times downstream of the IP shock (according to Figure 1).

change. When this source is drawn out (at $t_{nl} \approx 10$), the decay of MHD turbulence starts.

7. Discussion

In this section, we discuss the assumptions and approximations made in our analysis. We address the conditions for which Equations (1)–(2) are valid and we examine the relevance of a nonlinear time estimation (Equation (3)). First, in Equations (1)–(2), we assumed that (a) IP shocks propagate into a stationary medium, and (b) the spherical expansion of the solar wind does not radically influence our analysis. Although IP shocks are inherently non-stationary phenomena, the Rankine–Hugoniot conditions state that downstream plasma parameters can be calculated from the upstream ones for each particular IP shock. We suppose that constant upstream conditions with typical relative fluctuations ($\delta B/B_0 \sim 0.2$, $\delta v/v_A \lesssim 1$, and $\delta\rho/\rho_0 \sim 0.1$) do not influence overall

characteristics of propagating IP shocks. The solar wind contains many types of magnetic and plasma discontinuities that increase the level of fluctuations. The energy levels prior to and after them could be the same, but a jump in magnetic and velocity fields causes spikes in energy levels that are more distinct in the kinetic range (Figure 2). However, variations of the fluctuation level connected with waves and discontinuities in the upstream region would result in corresponding variations downstream. For this reason, we cannot say without doubt that the decreasing trend of the turbulent energy in Figure 3 is caused by its dissipation or by a decrease of the turbulent level of the yet unshocked plasma.

The superposed analysis solves this problem statistically. There is no reason for upstream solar wind plasma parameters and/or their variations to prefer an increasing or decreasing trend, thus the observed decrease of energy levels in time (Figures 4–5), though with a large scatter, could be attributed to a decay of the turbulent energy.

Regarding the assumption (b), where the spherical expansion is omitted, we examine the relevance of the downstream timescale in the analysis. In our set of IP shocks, the average K is $\approx$6 (Equation (2)), thus the average timescale of $t_{\rm sh}$ (Equation (1)) is roughly 60 hr. This implies that the plasma observed 10 hr after the IP shock was affected by this shock approximately at 0.7 au. The energy of fluctuations is generally larger there than at 1 au but it does not influence our results significantly because both upstream variations as well as enhanced variations downstream would decay with the same rate due to expansion.

In estimations of the nonlinear interaction time, we simplified the formula for $\tau_{\rm nl}$ (e.g., Matthaeus et al. 2014) and included only the Kolmogorov nonlinear time (the eddy turnover time), which is calculated from the velocity fluctuations. A similar method is often used in simulations (e.g., Franci et al. 2015). If the magnetic field fluctuations were not omitted, then $\tau_{\rm nl}$ would be smaller by a factor of $\sqrt{1+1/r_{\rm A}}$ (usually it would be $\lesssim$2). This factor would change the horizontal axis in Figure 6, but the decay rates would be conserved for $t_{\rm nl} \gg t_{\rm d}$.

Applications of these results to a general case of the turbulence decay in the solar wind require an assumption that basic parameters of turbulence are conserved across the shock. This was confirmed for density variations by Pitňa et al. (2016) and we did a similar analysis for the velocity and magnetic field variations. Since the results agree with those of Pitňa et al. (2016), we only list them here: (1) variations of the velocity and magnetic field increase by a factor of $\approx$20 across the IP shock; (2) the spectral indices are conserved; and (3) the break frequency between MHD and kinetic scales is related to the proton gyrostructure frequency. Moreover, we did not find any systematic trend of the increase of the kinetic and magnetic fractions of the turbulent energy. Alfvén ratios across the IP shock are in the range of 0.1–2 with an average value of about 0.7 in both upstream and downstream, as Figure 12 demonstrates. The average value roughly corresponds to that found in the pristine solar wind at 1 au (e.g., Matthaeus & Goldstein 1982; Marsch & Tu 1990; Bruno et al. 2007; Podesta et al. 2007; Salem et al. 2009; Chen et al. 2011, 2013).

Our superposed analysis revealed that both kinetic and magnetic components of the turbulent energy decay equally rapidly downstream of the IP shock. A conservation of the solar wind alfvénicity suggests that the dynamics of turbulence behind IP shocks is probably controlled by Alfvén wave effects.

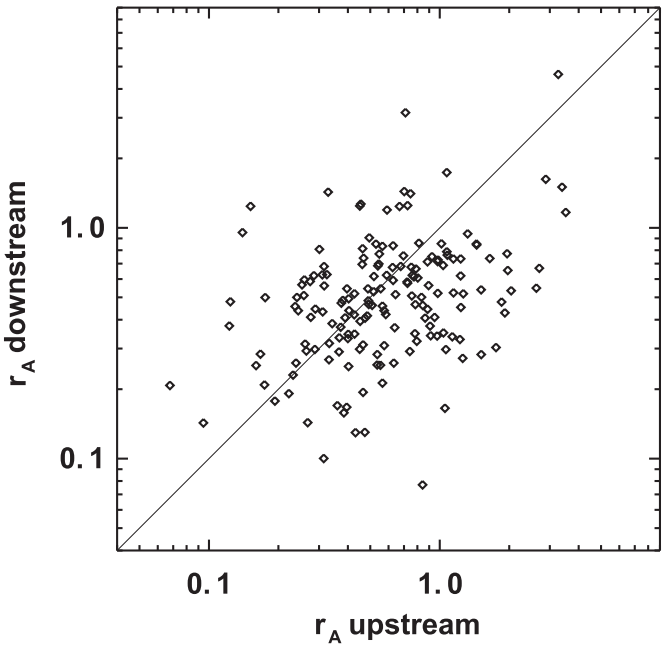

Figure 12. Alfvén ratio, $r_{\rm A}$, downstream IP shock as a function of $r_{\rm A}$ upstream.

However, we found that the power-law decay of both components does not start immediately after shock passage, but there is a time delay $t_{\rm d} \approx 10\, t_{\rm nl}$. We suggest that the kinetic processes initiated at the shock pump the energy to larger scales, and thus both the components of the turbulent energy as well as the Alfvén ratio are roughly constant through this interval. Further investigations are needed to determine if this process can be treated as an inverse turbulent cascade (Christensson et al. 2001) or if a description going out of the frame of classical turbulent theories could be applied. These theories expect that the plasma behavior can be explained in terms of an evolution of a relatively simple velocity distribution and its moments. However, Šafránková et al. (1994) have shown that the originally smooth distribution in front of the shock is broken into many beams at the ramp and these beams only gradually relax into a new downstream distribution.

Finally, the values of power-law exponents of the energy decay rates of kinetic and magnetic energies should be viewed in the context of the discussed limitations. However, we believe that their ratio $\simeq$1 is well supported with our analysis and it is in agreement with Biskamp & Müller (2000).

8. Conclusion

We have investigated the decay of kinetic and magnetic fluctuations downstream of IP shocks. We observed the power-law behavior of the energy decay profiles and we estimated the power-law exponents of both kinetic and magnetic energy decay rates. In detail, our analysis produces the following results.

1. A passage of the IP shock increases the power of fluctuations by a factor of 10 (e.g., Pitňa et al. 2016). This is true for both kinetic and magnetic components and their ratios are conserved in a statistical sense.

2. The enhanced level of fluctuations is roughly constant for $\approx 10\, t_{\rm nl}$. Our case study suggests that a level of kinetic fluctuations decreases in the course of this time.
3. The power-law decay starts at $t_{\rm nl} = t_{\rm d}$ and its rate is $n \simeq -1.2$ for both fractions of the turbulent energy that are similar to that theoretically derived (Biskamp 2003) and observed in MHD simulations (e.g., Matthaeus et al. 2003; Müller & Biskamp 2003).
4. The upstream level of fluctuations is reached in $\approx 80\, t_{\rm nl}$, which is an average of about 12 hr of the spacecraft time.

The phenomenological model that matches our superposed analysis contains an additional time constant $t_{\rm d}$ that determines when the turbulence starts to decay after the IP shock passage. We suggest that the reason for this delayed time is in the downstream kinetic processes connected with the IP shock microphysics.

The authors thank the Wind team for the magnetic field data. The BMSW data are available via http://aurora.troja.mff.cuni.cz/spektr-r/project/. This work was supported by the Czech Grant Agency under Contract 16-04956S. A.P. thanks to the Charles University Grant Agency through the project 1484217 and L.F. was funded by Fondazione Cassa di Risparmio di Firenze, through the project Giovani Ricercatori Protagonisti. The authors acknowledge valuable discussions with S. Landi.

Facilities: SRT, WIND.

References

Adhikari, L., Zank, G. P., Hunana, P., & Hu, Q. 2016a, JPhCS, 767, 012001
Adhikari, L., Zank, G. P., Hunana, P., & Hu, Q. 2016b, ApJ, 833, 218
Alexandrova, O., Carbone, V., Veltri, P., & Sorriso-Valvo, L. 2008, ApJ, 674, 1153
Alexandrova, O., Chen, C. H. K., Sorriso-Valvo, L., Horbury, T. S., & Bale, S. D. 2013, SSRv, 178, 101
Alexandrova, O., Saur, J., Lacombe, C., et al. 2009, PhRvL, 103, 165003
Bale, S. D., Kellogg, P. J., Mozer, F. S., Horbury, T. S., & Reme, H. 2005, PhRvL, 94, 215002
Balogh, A., & Treumann, R. A. 2013, Physics of Collisionless Shocks (1st ed.; New York: Springer)
Barnes, A. 1979, Hydromagnetic Waves and Turbulence in the Solar Wind (Amsterdam: North-Holland), 249–319
Bavassano, B., Dobrowolny, M., Mariani, F., & Ness, N. F. 1982, JGRA, 87, 3617
Belcher, J. W., & Davis, L., Jr. 1971, JGR, 76, 3534
Beresnyak, A. 2011, PhRvL, 106, 075001
Biskamp, D. 1993, Nonlinear Magnetohydrodynamics (Cambridge: Cambridge Univ. Press)
Biskamp, D. 2003, Magnetohydrodynamic Turbulence, 310 (Cambridge: Cambridge Univ. Press)
Biskamp, D., & Müller, W.-C. 1999, PhRvL, 83, 2195
Biskamp, D., & Müller, W.-C. 2000, PhPl, 7, 4889
Boldyrev, S., Perez, J. C., Borovsky, J. E., & Podesta, J. J. 2011, ApJL, 741, L19
Bruno, R., & Carbone, V. 2013, LRSP, 10, 2
Bruno, R., Carbone, V., Vörös, Z., et al. 2009, EM&P, 104, 101
Bruno, R., D'Amicis, R., Bavassano, B., Carbone, V., & Sorriso-Valvo, L. 2007, P&SS, 55, 2233
Chandran, B. D. G., Quataert, E., Howes, G. G., Xia, Q., & Pongkitiwanichakul, P. 2009, ApJ, 707, 1668
Chen, C. H. K., Bale, S. D., Salem, C. S., & Maruca, B. A. 2013, ApJ, 770, 125
Chen, C. H. K., Mallet, A., Yousef, T. A., Schekochihin, A. A., & Horbury, T. S. 2011, MNRAS, 415, 3219
Chen, C. H. K., Salem, C. S., Bonnell, J. W., Mozer, F. S., & Bale, S. D. 2012, PhRvL, 109, 035001
Chen, C. H. K., Sorriso-Valvo, L., Šafránková, J., & Němeček, Z. 2014, ApJL, 789, L8
Christensson, M., Hindmarsh, M., & Brandenburg, A. 2001, PhRvE, 64, 056405
Coburn, J. T., Smith, C. W., Vasquez, B. J., Stawarz, J. E., & Forman, M. A. 2012, ApJ, 754, 93
Coleman, P. J., Jr. 1968, ApJ, 153, 371
Cranmer, S. R., Field, G. B., & Kohl, J. L. 1999, ApJ, 518, 937
Cranmer, S. R., Panasyuk, A. V., & Kohl, J. L. 2008, ApJ, 678, 1480
Franci, L., Landi, S., Matteini, L., Verdini, A., & Hellinger, P. 2015, ApJ, 812, 21
Goldreich, P., & Sridhar, S. 1995, ApJ, 438, 763
Goldstein, M. L., Roberts, D. A., & Matthaeus, W. H. 1995, ARA&A, 33, 283
Grappin, R., & Müller, W.-C. 2010, PhRvE, 82, 026406
Hefti, S., Grünwaldt, H., Ipavich, F. M., et al. 1998, JGR, 103, 29697
Hellinger, P., TráVníček, P. M., Štverák, Š, Matteini, L., & Velli, M. 2013, JGRA, 118, 1351
Hollweg, J. V. 1978, RvGSP, 16, 689
Hollweg, J. V. 1986, JGR, 91, 4111
Horbury, T. S., Balogh, A., Forsyth, R. J., & Smith, E. J. 1995, GeoRL, 22, 3405
Horbury, T. S., Forman, M. A., & Oughton, S. 2005, PPCF, 47, B703
Howes, G. G. 2015, RSPTA, 373, 20140145
Hu, Q., Zank, G. P., Li, G., & Ao, X. 2013, in AIP Conf. Proc. 1539, Solar Wind 13, ed. G. P. Zank et al. (Melville, NY: AIP), 175
Kiyani, K. H., Chapman, S. C., Sahraoui, F., et al. 2013, ApJ, 763, 10
Lamarche, L. J., Vasquez, B. J., & Smith, C. W. 2014, JGRA, 119, 3267
Leamon, R. J., Smith, C. W., Ness, N. F., Matthaeus, W. H., & Wong, H. K. 1998, JGRA, 103, 4775
Lee, L. C., Wu, C. S., & Hu, X. W. 1986, GeoRL, 13, 209
Lepping, R. P., Acũna, M. H., Burlaga, L. F., et al. 1995, SSRv, 71, 207
Linkmann, M. F., Berera, A., McComb, W. D., & McKay, M. E. 2015, PhRvL, 114, 235001
Lu, Q., Hu, Q., & Zank, G. P. 2009, ApJ, 706, 687
Luttrell, A., Richter, A. K., Rosenbauer, H., & Neubauer, F. M. 1984, AdSpR, 4, 327
Marsch, E., Muehlhaeuser, K. H., Rosenbauer, H., & Schwenn, R. 1983, JGR, 88, 2982
Marsch, E., & Tu, C.-Y. 1990, JGR, 95, 8211
Matthaeus, W. H., Dmitruk, P., Smith, D., Ghosh, S., & Oughton, S. 2003, GeoRL, 30, 2104
Matthaeus, W. H., Ghosh, S., Oughton, S., & Roberts, D. A. 1996, JGR, 101, 7619
Matthaeus, W. H., & Goldstein, M. L. 1982, JGR, 87, 6011
Matthaeus, W. H., Goldstein, M. L., & Roberts, D. A. 1990, JGR, 95, 20673
Matthaeus, W. H., Goldstein, M. L., & Smith, C. 1982, PhRvL, 48, 1256
Matthaeus, W. H., Oughton, S., Ghosh, S., & Hossain, M. 1998, PhRvL, 81, 2056
Matthaeus, W. H., Oughton, S., Osman, K. T., et al. 2014, ApJ, 790, 155
Matthaeus, W. H., & Zhou, Y. 1989, PhFlB, 1, 1929
Müller, W.-C., & Biskamp, D. 2003, in Turbulence and Magnetic Fields in Astrophysics, Vol. 614, ed. E. Falgarone & T. Passot (Berlin: Springer), 3
Müller, W.-C., & Grappin, R. 2005, PhRvL, 95, 114502
Ogilvie, K. W., Chornay, D. J., Fritzenreiter, R. J., et al. 1995, SSRv, 71 55
Oughton, S., Wan, M., Servidio, S., & Matthaeus, W. H. 2013, ApJ, 768, 10
Parker, E. N. 1965, SSRv, 4, 666
Pitňa, A., Šafránková, J., Němeček, Z., et al. 2016, ApJ, 819, 41
Podesta, J. J., Roberts, D. A., & Goldstein, M. L. 2007, ApJ, 664, 543
Podesta, J. J., & Borovsky, J. E. 2010, PhPl, 17, 112905
Podesta, J. J., Roberts, D. A., & Goldstein, M. L. 2006, JGRA, 111, A10109
Riazantseva, M. O., Budaev, V. P., Zelenyi, L. M., et al. 2015, RSPTA, 373, 20140146
Šafránková, J., Němeček, Z., Němec, F., et al. 2015, ApJ, 803, 107
Šafránková, J., Němeček, Z., Němec, F., et al. 2016, ApJ, 825, 121
Šafránková, J., Němeček, Z., Přech, L., et al. 2013a, SSRv, 175, 165
Šafránková, J., Němeček, Z., Přech, L., & Zastenker, G. N. 2013b, PhRvL, 110, 025004
Sahraoui, F., Goldstein, M. L., Robert, P., & Khotyaintsev, Y. V. 2009, PhRvL, 102, 231102
Salem, C., Mangeney, A., Bale, S. D., & Veltri, P. 2009, ApJ, 702, 537
Salem, C., Mangeney, A., Bale, S. D., Veltri, P., & Bruno, R. 2007, in AIP Conf. Proc. 932, Turbulence and Nonlinear Processes in Astrophysical Plasmas, ed. D. Shaikh & G. P. Zank (Melville, NY: AIP), 75
Salem, C. S., Howes, G. G., Sundkvist, D., et al. 2012, ApJL, 745, L9
Scholer, M., Shinohara, I., & Matsukiyo, S. 2003, JGRA, 108, 1014
Servidio, S., Matthaeus, W. H., & Dmitruk, P. 2008, PhRvL, 100, 095005
Smith, C. W., Hamilton, K., Vasquez, B. J., & Leamon, R. J. 2006, ApJL, 645, L85

Taylor, G. 1938, RSPSA, 164, 476
Torrence, C., & Compo, G. P. 1998, BAMS, 79, 61
Vasquez, B. J., Smith, C. W., Hamilton, K., MacBride, B. T., & Leamon, R. J. 2007, JGRA, 112, A07101
Verma, M. K., Roberts, D. A., & Goldstein, M. L. 1995, JGR, 100, 19839
von Steiger, R., Geiss, J., Gloeckler, G., & Galvin, A. B. 1995, SSRv, 72, 71
Šafránková, J., Němeček, Z., & Santolík, O. 1994, AdSpR, 14, 31
Webb, D. F., & Howard, T. A. 2012, LRSP, 9, 3
Zank, G. P., Dosch, A., Hunana, P., et al. 2012, ApJ, 745, 35
Zank, G. P., & Matthaeus, W. H. 1993, PhFl, 5, 257
Zank, G. P., Zhou, Y., Matthaeus, W. H., & Rice, W. K. M. 2002, PhFl, 14, 3766
Zastenker, G. N., Šafránková, J., Němeček, Z., et al. 2013, CosRe, 51, 78
Zhou, Y., Matthaeus, W. H., & Dmitruk, P. 2004, RvMP, 76, 1015